Brain Imaging and Behavior (2019) 13:1333–1351
https://doi.org/10.1007/s11682-018-9949-2

ORIGINAL RESEARCH

Overall survival time prediction for high-grade glioma patients based on large-scale brain functional networks

Luyan Liu[1,2] · Han Zhang[2] · Jinsong Wu[3,4,5] · Zhengda Yu[3] · Xiaobo Chen[2] · Islem Rekik[2,6] · Qian Wang[1] · Junfeng Lu[3,4,5] · Dinggang Shen[2,7]

Published online: 28 August 2018

Abstract

High-grade glioma (HGG) is a lethal cancer with poor outcome. Accurate preoperative overall survival (OS) time prediction for HGG patients is crucial for treatment planning. Traditional presurgical and noninvasive OS prediction studies have used *radiomics* features at the local lesion area based on the magnetic resonance images (MRI). However, the highly complex lesion MRI appearance may have large individual variability, which could impede accurate individualized OS prediction. In this paper, we propose a novel concept, namely brain *connectomics*-based OS prediction. It is based on presurgical resting-state functional MRI (rs-fMRI) and the non-local, large-scale brain functional networks where the global and systemic prognostic features rather than the local lesion appearance are used to predict OS. We propose that the connectomics features could capture tumor-induced network-level alterations that are associated with prognosis. We construct both *low-order* (by means of sparse representation with regional rs-fMRI signals) and *high-order* functional connectivity (FC) networks (characterizing more complex multi-regional relationship by synchronized dynamics FC time courses). Then, we conduct a graph-theoretic analysis on both networks for a jointly, machine-learning-based individualized OS prediction. Based on a preliminary dataset ($N = 34$ with bad OS, mean OS, ~400 days; $N = 34$ with good OS, mean OS, ~1030 days), we achieve a promising OS prediction accuracy (86.8%) on separating the individuals with bad OS from those with good OS. However, if using only conventionally derived descriptive features (e.g., age and tumor characteristics), the accuracy is low (63.2%). Our study highlights the importance of the rs-fMRI and brain functional connectomics for treatment planning.

Keywords Survival · Prognosis · Glioma · Functional connectivity · Brain network · Connectomics · Machine learning

Luyan Liu and Han Zhang contributed equally to this work.

Electronic supplementary material The online version of this article (https://doi.org/10.1007/s11682-018-9949-2) contains supplementary material, which is available to authorized users.

✉ Qian Wang
wang.qian@sjtu.edu.cn

✉ Junfeng Lu
hlujf@126.com

✉ Dinggang Shen
dgshen@med.unc.edu

[1] Med-X Research Institute, School of Biomedical Engineering, Shanghai Jiao Tong University, 1954 Huashan Road, Shanghai 200030, China

[2] Department of Radiology and BRIC, University of North Carolina at Chapel Hill, Chapel Hill, NC, USA

[3] Glioma Surgery Division, Neurosurgery Department of Huashan Hospital, Fudan University, Shanghai 200040, China

[4] Shanghai Key Lab of Medical Image Computing and Computer-Assisted Intervention, Shanghai 200040, China

[5] Neurosurgery Department of Huashan Hospital, 12 Wulumuqi Zhong Road, Shanghai 200040, China

[6] BASIRA Lab, CVIP Group, School of Science and Engineering, Computing, University of Dundee, Dundee, UK

[7] Department of Brain and Cognitive Engineering, Korea University, Seoul 02841, Republic of Korea

Introduction

Gliomas account for ~70% of adult primary brain tumors (Ricard et al. 2012). The prognosis of gliomas is generally poor, compared with other types of brain tumors, and is traditionally considered dependent on patients' age and physical status, tumor histopathology and location (Ostrom et al. 2013), surgical treatment (e.g., extent of resection) (Smith et al. 2008; Jain et al. 2014), post-surgical adjuvant therapy (Grossman et al. 2010), as well as several molecular and genetic indicators (Macyszyn et al. 2016). World Health Organization (WHO) grade is a commonly used grading system for gliomas (Louis et al. 2007), where high-grade gliomas (HGGs), including grade-III (e.g., anaplastic astrocytoma) and IV (glioblastoma multiforme) gliomas, are believed to have a faster growth rate and worse outcome compared with WHO grade-II gliomas (Stylli et al. 2005). The median survival time of anaplastic astrocytoma and glioblastoma is 2–3 years and 1 year, respectively. Accurate preoperative overall survival (OS) time prediction for patients with HGGs is crucial for individualized treatment planning. However, in clinical practice, the OS of HGG patients may differ significantly from case to case even though the patients have the same tumor grade and receive similar treatments (Sawaya et al. 1998; Legler et al. 1999). While challenging, progress has been made toward accurate pre-surgical OS prediction for HGG patients based on various non-invasive brain imaging techniques.

Previously, researchers have utilized non-invasive structural and functional preoperative neuroimaging techniques to *1)* search for molecular biomarkers of gliomas (Kickingereder et al. 2016a; Itakura et al. 2015; Grabner et al. 2016), *2)* model tumor growth dynamics (Stensjøen et al. 2015), and *3)* differentiate glioma subtypes (Collet et al. 2015). These studies have directly or indirectly contributed to survival time prediction. Moreover, recent efforts have been made to directly characterize the association between elaborately engineered imaging phenotypic features and the glioma patients' OS (Cui et al. 2015; Kickingereder et al. 2016b), as radio-diagnosticians and neuro-oncologists have leveraged such information for surgical planning for decades (Wang et al. 2015b; Pope et al. 2005). Compared to the prognostic genomic or molecular pathology information (Phillips et al. 2006), preoperative brain images are easier to acquire, as they introduce no or minimal (with contrast agency injection only) invasiveness. On the other hand, imaging phenotypic profiles extracted from the glioma images are more objective and comprehensive compared to the conventional descriptive features (e.g., patient's age, daily life performance score and physical status). In previous imaging-based OS prediction studies, *radiomics* features have been widely used, where numerous quantitative image descriptors are extracted from the lesion areas based on brain structural magnetic resonance images (MRI, including T1-weighted, T2-weighted, and T2-fluid attenuated inversion recovery (T2-FLAIR) imaging with/without contrast enhancement). This type of methods takes advantage of the high spatial resolution and abundant tissue contrast from the structure MRI (Gillies et al. 2015; Macyszyn et al. 2016; Mazurowski et al. 2014; Kickingereder et al. 2016b; Cui et al. 2015). Additionally, there are survival prediction studies using diffusion-weighted imaging (DWI) (Zacharaki et al. 2012; Saksena et al. 2010), perfusion weighted imaging (PWI) (Bisdas et al. 2009; Law et al. 2008; Jain et al. 2014), and positron emission tomography (PET) (Chen et al. 2007), which have shown complementary prognostic values besides structural MRI.

A common analysis strategy in the aforementioned studies is making prognosis prediction based on attributes of the tumors (e.g., tumor size, shape, contrast, and location) and/or manually (or automatically) engineered complex image descriptors (e.g., texture, inhomogeneity and intensity distributions) inside or nearby the tumors. Although it is straightforward, a potential issue is that all these *local features* highly depend on the tumor appearance, which could largely vary across different individuals. With such wider distributions of the predictive features, detecting true OS-associated radiomics indicators could be difficult. Moreover, these local features are difficult to be directly compared among different patients with distinct tumor sizes, shapes and/or locations. To tackle these issues, most of the previous studies have adopted a group-level statistical analysis to stratify the survival curves at the population level, i.e., constructing a group-level OS prediction model (Jain et al. 2014; Kickingereder et al. 2016b; Cui et al. 2015; Zacharaki et al. 2012; Saksena et al. 2010; Lacroix et al. 2001). With the statistically significant level only, findings from these studies cannot be easily utilized for modeling *individual* prognosis. In addition, many radiomics-based studies have adopted only a limited number of manually-engineered features according to the researchers' best prior knowledge, but inevitably neglecting other potentially useful features. This could lead to inconsistent findings across different studies. In other words, different studies have used different imaging features and their findings could not be comparable. For example, the extent of necrosis inside the gliomas was found negatively related to survival time (Pope et al. 2005), while a positive relationship between them was also reported (Maldaun et al. 2004). In another example, the mass effect of the tumor was found to be not significantly associated with survival time (Lacroix et al. 2001), but it was also suggested as one of the two most important prognostic indicators (Zacharaki et al. 2012). Besides, human interference in focal lesion delineation, e.g., manual tumor segmentation or para-tumor edema area delineation, may further introduce biases.

In addition to extract local *radiomics* features from the lesion areas, the whole-brain *connectomics* features extracted beyond the lesion areas have been recently proposed to be

useful for clinical neuroscience studies, where the functional connectomics can be extracted from the "normal appearing" brain regions based on resting-state functional MRI (rs-fMRI) (Glasser et al. 2016; Sporns et al. 2004; Smith et al. 2011). With rs-fMRI, brain spontaneous activity can be measured by blood oxygen level-dependent (BOLD) signal and, according to their temporal synchronization between two spatially remoted brain regions, functional connectivity (FC) can be further calculated, measuring functional relationships between the two regions (Biswal et al. 1995; Horwitz et al. 1987; Horwitz 2003). By calculating FCs for all pairs of the brain regions, a large-scale whole-brain functional network (functional connectomics) can be constructed, and the network properties can be quantified using graph-theoretic analysis (Van Den Heuvel and Pol 2010; Rubinov and Sporns 2010; Bullmore and Sporns 2009; Wee et al. 2012). Brain functional connectomics features have been extensively used to reveal abnormalities caused by various neurological and psychiatric diseases (Rosazza and Minati 2011; Fox and Greicius 2010), including brain tumors (Hart et al. 2016a, b; Aerts et al. 2016; van Dellen et al. 2013; Xu et al. 2013; Huang et al. 2014). These studies have demonstrated that local lesion (s) could potentially have a much wider influence on the large-scale brain networks, causing network topographical changes and other system-level consequences (Wang et al. 2009b; Wang et al. 2010; Zhang et al. 2009; Tijms et al. 2013).

Similarly, gliomas may also lead to topographical alterations to the whole-brain FC connectomics (Hart et al. 2016a, b; Aerts et al. 2016; Ghumman et al. 2016; Bartolomei et al. 2006; Bosma et al. 2009; Cochereau et al. 2016). It is probable that different gliomas could cause distinct influences to the brain functional connectomics, resulting in different aftermaths from multi-dimensional behavioral abnormalities to varied survival time. Glioma entity can be regarded as a focal pathological attack on the whole brain connectomics. If it is more invasive (i.e., penetrating/involving more brain regions and/or growing faster), it may not only affect local contrast-enhanced area but also cause more catastrophic consequences involving wider networks (i.e., the tumor effect may extend to normal appearing brain areas or even counter-lateral hemisphere). In addition, it may further lead to more impaired cognitive abilities or behavioral performance, eventually causing a shorter OS. On the contrary, if the tumor is less invasive, such effects could be relatively local; the whole network could be less affected, and the patient could have better daily life performance, largely reserved cognitive ability, and a longer OS.

In a short conference paper, we have demonstrated that the traditional Pearson's correlation-based FC network and another traditional structural network (from DWI) could be jointly used for OS stratification and found that the FC network contributed more in this task (Liu et al. 2016). However, only 75% accuracy was achieved, which is not satisfactory for a clinical study. The reason could be the heavy noise in the rs-fMRI data from the diseased brains and the insensitivity of traditional FC-based networks on the OS stratification. In this paper, we propose a novel method, namely brain connectomics-based OS prediction. It is based on non-invasive, increasingly adopted presurgical rs-fMRI and non-local, large-scale brain networks where global and systemic prognostic features rather than local lesion appearance features are utilized as prognostic features. Instead of relying on the structural MRI, we leverage functional MRI during resting state to characterize intrinsic brain functional organizations and build functional connectomics that could capture tumor-induced network-level alterations associated with prognosis. We use a single-site-based HGG dataset with long follow-up time (until the OS information were collected from most of the patients) and research-dedicated rs-fMRI data to investigate whether it is feasible to conduct presurgical OS prediction in an individualized manner based on the global topology of the large-scale brain networks. Different from our previous study (Liu et al. 2016), we construct both robust *low-order* (by means of sparse representation with regional BOLD rs-fMRI time series for better noise suppression) and *high-order* FC networks (an advanced brain network construction method that characterizes more complex and sensitive multi-regional interactions by synchronization of the FC dynamics) to better capture the tumor-induced alterations. Then, we extract features from both networks with graph-theoretic analysis for a joint machine-learning-based individualized OS prediction.

Materials and methods

Participants

In this study, 148 patients with primary HGGs were initially included retrospectively from our glioma patients multimodal brain imaging dataset built since 2010. They were all untreated when neuroimaging data were collected. All clinical and imaging datasets were collected from a single site (to rule out the multi-center effect) based on the Huashan Glioma Tissue Bank (GTB) Registry (Aibaidula et al. 2015), which was approved by the Huashan Institutional Review Board. All the patients provided written informed consent prior to the recruitment. From the diagnostic contrast-enhanced T1-weighted images, all patients showed enhanced tumors that indicated HGGs, as confirmed by a histopathological technique. To maximally reduce the confounding effect of surgery and post-surgery treatment, we treated all patients equally and consistently according to the clinical guideline for HGG. Specifically, we included the subjects with maximal safe resection (confirmed by postoperative follow-up MRI) via craniotomy by the same neurosurgeon (JW) to ensure the consistency of surgical treatment for fair outcome prediction. All the patients received concurrent high conformal radiation and

chemotherapy with Temozolomide followed by six cycles of Temozolomide in accordance with the Stupp's regimen (Stupp et al. 2002). Each patient received fractionated focal irradiation in daily fractions of 2 Gy given 5 days per week for 6 weeks (equals a total dose of 60 Gy).

All patients received regular follow-ups every three months following discharge. None of them developed permanent motor or language deficits. Patients' family members reported any vital event, such as death, based on which we calculated the OS time. Patients with any of the following situations were excluded: *1)* excessive head motion (> 2 mm in translation or > 2 degrees in rotation along any direction) during the rs-fMRI scan or other imaging artifacts in T1 images, *2)* inadequate follow-up time to determine long or short OS, *3)* obvious irrelevant death causes (e.g., suicide), and *4)* excessive tumor-induced brain deformation which caused misalignment during rs-fMRI registration as determined by a consensus of three raters (HZ, JL, and LL). OS time was defined by the duration between the date of operation and the date of death. We counted the death caused by gliomas and the death caused by other unclear reasons. Due to the limited sample size, we treated the OS prediction task as a much easier two-class classification problem (i.e., short vs. long OS), rather than a more realistic regression problem. This is because the regression task generally requires more sample size to fit the regression model. The current study can be regarded as a pilot study or a testbed to investigate the feasibility of FC-based OS prediction. In addition, the patients who were still alive according to the last follow-up but had already lived longer than the cutoff were labeled as long OS. The threshold between long OS and short OS was chosen to be 650 days, which is a median OS for adult HGG patients (Wu et al. 2007). That is, the patients who died within 650 days after surgery are labeled as short (or bad) OS, and those who died after 650 days or lived longer than 650 days are defined as long (or good) OS.

We removed 14 (9.46%) patients due to excessive head motion and 7 (4.7%) patients due to imaging artifacts. There were 4 patients with both excessive head motion and imaging artifacts, so the total number of the removed subjects based on preprocessing quality is 17 (11.5%). Of note, other 6 subjects were also excluded because that the reason of death was not caused by HGGs, and there are 57 patients excluded because there was no information about the date of their death or they only had short follow-ups, making us difficult to determine their OS. Finally, 68 patients were remained, with 34 having short OS and the other 34 having long OS. Between the two groups, there is no significant difference in pre-operatively assessed tumor volume ($p = 0.55$), extension of tumor resection ($p = 0.22$), or the ways of post-surgical treatments received ($p = 0.82$). Detailed subject information is summarized in Table 1. In addition, tumor locations are similar for the two groups ($p = 0.27$, see also Electronic Supplementary Materials for the tumor probability maps of both groups). There are no significant group differences in gender, hemisphere involved, and mass effect caused by tumors. However, ages of the short OS group are significantly older than that of the long OS group ($p = 0.04$). Tumor WHO grade and histopathological subtypes have significant group differences ($p = 0.01$), with the short OS group having more glioblastoma patients; however, this factor alone was not able to make individual prognosis (see the result from OS prediction using traditional features).

MRI acquisitions

For each patient, a whole-brain, high-resolution, contrast-enhanced 3D-MPRAGE (magnetization-prepared rapid-gradient echo) T1 MRI and an 8-min EPI (echo-planar imaging) rs-fMRI data were acquired pre-operatively with a 3.0-Tesla scanner (MAGNETOM Verio, Siemens Healthcare, Germany) at Huashan Hospital. The imaging parameters of the T1-MRI are: TR (repetition time) = 1900 ms; TE (echo time) = 2.3 ms; FA (flip angle) = 9°; FOV (field of view) = 240 × 240 mm^2; matrix size = 256 × 215; and slice thickness = 1 mm. The imaging parameters of the rs-fMRI are: TR = 2000 ms; TE = 35 ms; FA = 90°; number of slices = 33; slice thickness = 4 mm; inter-slice gap = 0; FOV = 210 × 210 mm^2; matrix size = 64 × 64; voxel size = 3.4 × 3.4 × 4 mm^3; and number of acquisitions = 240. The contrast-enhanced T1 MRI was used to preoperatively assess tumor grade and to guide rs-fMRI registration. Of note, our single-center-based data might unavoidably narrow the applicable scenarios; however, we believe that the consistent settings could improve technical validity and control the confounding effects. In the future, data from different sites with different imaging protocols can help to learn a predictive model with better generalizability.

Data preprocessing

Data preprocessing was carried out using SPM8 (http://www.fil.ion.ucl.ac.uk/spm/), which includes the following steps: *1)* discard the first 5 volumes for scanner calibration, *2)* correct for slice acquisition timing and head motion, *3)* spatial registration to the standard Montreal Neurological Institute (MNI) space by using the deformation field obtained from "New Segment" (an extension of SPM's default "Unified Segmentation", which obtains more robust brain tissue segmentation results via a group-wise registration algorithm (Ashburner and Friston 2005)) and DARTEL (a fast diffeomorphic registration algorithm which achieves better performance on lesion brain registration (Ashburner 2007) using group-wise, iteration-based algorithm) to the co-registered T1-MRI, *4)* spatial smoothing using a Gaussian kernel with FWHM (full-width-at-half-maximum) of 6×6×6 mm^3, *5)* temporal linear trend removal, temporal band-pass filtering (0.01–0.08 Hz), and *6)* regress out

Table 1 Demographics, clinical and pathological characteristics of all the 68 subjects

Variable	Short OS group	Long OS group	p
Age (years)			0.04*
Mean ± std	55.0±14.0	47.7±14.2	
Range	16–74	18–74	
Gender — male no. (%)	25 (73.5)	23 (67.7)	0.81
Hemisphere — no. (%)			0.33
Left	25 (73.5)	25 (73.5)	
Right	7 (20.6)	9 (26.5)	
Bilateral	2 (5.9)	0 (0)	
Main location[a] — no. (%)			0.27
Occipital	2 (5.9)	2 (5.9)	
Temporal	12 (35.3)	8 (23.5)	
Parietal	3 (8.8)	4 (11.8)	
Frontal	12 (35.3)	19 (55.9)	
Insula	5 (14.7)	1 (2.9)	
Extension of distortion[b] — no. (%)			0.26
0	3 (8.8)	6 (17.7)	
1	6 (17.7)	9 (26.5)	
2	19 (55.9)	11 (32.4)	
3	6 (17.7)	8 (23.5)	
WHO, Histology — no. (%)			<0.01*, 0.01*
III: Anaplastic Astrocytomas	7 (20.6)	11 (32.4)	
III: Anaplastic Oligodendrogliomas	1 (2.9)	8 (23.5)	
III: Anaplastic Ependymomas	0 (0)	1 (2.9)	
IV: Glioblastoma	26 (76.5)	14 (41.2)	
Tumor size (preoperative) — cm^3			0.55
Mean ± std	50.5±36.3	56.3±43.1	
Range	1.7–200	3.1–178.0	
Epilepsy — no. (%)	9 (26.5)	18 (52.9)	0.05*
Tumor distribution[c] — no. (%)			0.43
1	15 (44.1)	14 (41.2)	
2	15 (44.1)	12 (35.3)	
3	4 (11.8)	8 (23.5)	
Overall survival — days			–
Mean ± std	401.4±158.0	1031.7±273.3	
Range	118–649	654–1653	

[a] Main location is a region where the tumor mainly located

[b] Extension of distortion describes the distortion of normal brain structure caused by tumor using a four-grade scale ranging from 0 to 3, as assessed by three researchers (HZ, JW and JL) independently (determined by majority rating when consensus could not be reached) based on contrast-enhanced T1 MRI, where 0 means almost no distortion observed, 3 indicates large distortion (but not affecting image registration) in T1 MRI

[c] Tumor distribution, a three-grade scale ranging from 1 to 3, denotes the number of different brain lobes (i.e., 5 different lobes used in this study; see "main location") with tumor (e.g., 1 denotes that the tumor appears only in one brain region) as assessed by HZ, JW and JL with consensus

*indicates a significant difference between the short and the long OS groups (i.e., $p < 0.05$)

nuisance signals including the head motion profiles (*Friston-24* model) and other physiological noises (averaged white-matter signals and averaged cerebrospinal-fluid signals). Of note, the tumor effect on the registration was minimized by the above strategy using "New Segment". The registered T1 images were visually checked to ensure no excessive distortion in the registered T1 images of all subjects. It should also be noted that spatial smoothing might not be necessary for the region-wise FC study (Alakorkko et al. 2017). We did not exclude this step because it is a common practice in the

well-known rs-fMRI analysis toolboxes and it can increase the signal-to-noise ratio of the rs-fMRI data (Mikl et al. 2008).

The preprocessed rs-fMRI data were used to extract functional connectomics. A key point is an accurate construction and comprehensive presentations of the brain functional networks. Therefore, we used different node/edge definitions to construct the brain networks from two different perspectives. Most of the brain functional network studies have treated brain regions as nodes, and the FC between each pair of the nodes as an edge (Smith et al. 2011). This network is called by us *low-order* FC network. Recently, we proposed a *high-order* brain network construction method based on "correlation of correlations", which further calculates the temporal synchronization among the dynamic FC (Hutchison et al. 2013; Damaraju et al. 2014; Wee et al. 2016) time series (i.e., time-varying FC, rather than traditional static FC). We have shown that the high-order brain network provided complementary information to the traditional low-order functional network in early Alzheimer's disease detection (Chen et al. 2016a, b, 2017). In such a high-order network, a "hyper-node" consists of two brain regions, and a "hyper-edge" characterizes a quadruple high-order relationship among a set of four (two brain region pairs) brain regions (Chen et al. 2016a, b; Zhang et al. 2017a). In this paper, we adopt the Automated Anatomical Labeling (AAL) template (Tzourio-Mazoyer et al. 2002) to define 116 brain regions; each region's mean rs-fMRI time course was extracted for the subsequent network construction. Of note, the AAL atlas was generated based on the anatomical landmarks from a single subject, which may not correspond to the real "functional border" of the brain regions. An alternative way is to use a brain parcellation directly derived from rs-fMRI based on FC boundary, as described in Gordon et al. (2016), where the FC boundary-based atlas was proposed to be better than other popular brain atlases. The reasons for choosing the AAL in this study rather than other atlases are provided below. First, a recent study on the influence of different templates on the properties of the complex brain network indicated that different parcellation scales might not affect major network properties such as small-worldness (Zalesky et al. 2010). Specifically, the estimates of various network organization properties (e.g., clustering, shortest path length, and efficiency) are consistent across different atlases with comparable resolution (Zalesky et al. 2010). However, it is noted that other studies hold a different opinion (Wang et al. 2009a; Fornito et al. 2010; Rubinov and Sporns 2010), indicating that different atlases could affect the result of network-based OS prediction. Second, the AAL parcellation is based on the borders constrained by the major sulcus and gyrus, which can be largely well aligned across subjects. Third, the AAL contains an optimal number of brain regions that could make each region large enough to compensate possible tumor-induced lesion effect or distortion. The appropriate total brain region number (~100) also reduces the computational load of the high-order FC networks used in this paper, as the high-order nodes increase dramatically (Chen et al. 2016a, b; Zhang et al. 2017a). Finally, compared to other atlases, AAL contains both cortical, subcortical and cerebellar regions, which could be equally important for OS prediction. Future work is desired to further investigate the influence of different brain parcellation atlases on the OS prediction.

Robust sparse representation-based low-order brain connectomics

Sparse representation was used to construct low-order brain networks, which is a commonly used method for capturing interactions between one brain region and all other brain regions while ensuring the sparsity of whole-brain connectivity pattern. However, when applying the commonly used sparse representation algorithms to the data with brain tumors, lesions could make the representation problematic (i.e., the result can be largely affected by the lesion-induced noise). We proposed a robust method by using a non-squared data-fitting term in the loss function to suppress the noise induced by the tumors. In addition, we further penalized noisy/weak connections while preserving strong/putative connections by explicitly using Pearson's correlation-based FC strength as a weight in the sparse regularization term. Please refer to Yu et al. (2016b) and the Electronic Supplementary Materials for details. Of note, this network construction strategy is particularly suitable for lesion brain studies.

FC dynamics-based high-order brain connectomics

First, a sliding-window approach was adopted to construct dynamic FC between each pair of brain regions, with both the window width and step size determined by cross-validation. Second, the resultant dynamic FC time series were used to calculate the second round of Pearson's correlations which measure temporal synchronization of the FC dynamics. Theoretically, 116 brain regions will form a 116×116 low-order FC matrix and a 6670×6670 (i.e., $C_{116}^2 \times C_{116}^2$, where C denotes combination operation) high-order FC matrix. In practice, we adopted hierarchical clustering on the subject-concatenated dynamic FC time series to group the similarly fluctuated dynamic FCs into the same cluster (with the cluster number chosen as 600 according to cross-validation performance, as described later) to reduce the data dimensionality from C_{6670}^2 to C_{600}^2. The cluster centers are treated as hyper-nodes, and the pair-wise correlations among them are the hyper-edges.

Graph-theoretic analysis-based connectomics feature extraction

From both brain networks, we calculated four types of metrics that characterize various aspects of network properties (Rubinov and Sporns 2010) using GRETNA (Wang et al. 2015a). All the features are extracted from the weighted networks. They are: *1)* degree, defined by summarizing all connectivity strengths to each node; *2)* small-worldness, including local clustering coefficient (measuring local connectivity of a node's neighbors) and the shortest path length (characterizing overall communication cost between one node to all others); *3)* network efficiency, measuring how efficient information is exchanged within a network globally (global efficiency) and locally (local efficiency); and *4)* betweenness centrality, quantifying the importance of each node to the whole network, defined by the fraction of the shortest paths passing through this node to all shortest paths that do not pass through it.

Machine-learning-based overall survival prediction

Features from both types of functional connectomics were used to train two support vector machine (SVM) models (Cortes and Vapnik 1995) separately, and their respective classification scores were fused by weighted averaging to produce the final OS prediction result (Chen et al. 2016a; Fan et al. 2008). In the training process, we conducted feature selection using LASSO (Least Absolute Shrinkage and Selection Operator) to identify a small number of informative features. Besides the connectomics features, we also included 13 traditional clinical features (including demographic variables, i.e., age and gender; and tumor-related features, i.e., tumor size, main location and distribution, WHO grade and histopathology type; as well as preoperative symptom, i.e., epilepsy, see Electronic Supplementary Materials for details) as they have been previously demonstrated to be associated with the prognosis. We did not include preoperative Karnofsky Performance Status (KPS) scores since all patients had KPS > 80 (with most of them being >90), causing a ceiling effect with little difference between the two groups ($p > 0.99$). We included neither post-operative imaging nor post-operative clinical features because our study here was aimed to investigate the feasibility of preoperative prediction. Nevertheless, we by no means think that surgical and post-surgical treatments are irrelevant to OS (Rahman et al. 2017). A total of 709 features (6 metrics × 116 regions +13 traditional features) were extracted for each network per subject. The entire OS prediction framework is depicted in Fig. 1.

Prediction model evaluation and comparisons with other methods

The generalization ability of our OS prediction model was evaluated by a nested cross-validation strategy, with leave-one-out cross-validation (LOOCV) used in the outer loop and 10-fold cross-validation used in the inner loop (Chen et al. 2016a). Specifically, during each LOOCV, one subject was selected for testing, and the remaining 67 subjects were used as training samples in the inner 10-fold cross validation for parameter optimization. The parameters and their predetermined ranges are window width $\in[20, 30, \cdots, 100]$ and stepping size $\in[1, 2, 4, 8, 10]$ for dynamic FC calculation, the number of clusters $\in$ [100, 200, … 700] for high-order connectomics calculation, the parameter $\lambda\in[0.1, 0.2, \cdots, 0.9]$for feature selection with LASSO, two hyperparameters $C \in[2^{-9}, 2^{-8}, \cdots, 2^{9}]$ for the two SVMs, and the weight $\alpha \in[0.1, 0.2, \cdots, 0.9]$ for result fusion. The final optimized values are: window width = 30, stepping size = 2, cluster number = 600, $\lambda = 0.7$, $C = 2^{-8}$, and $\alpha = 0.3$. The testing subject was then fed into the trained classification model for generating the prediction result. This procedure was conducted 68 times until every subject had been selected once. We then calculated the accuracy (ACC), sensitivity (SEN) and specificity (SPE) by treating the short OS samples as positive samples and the long OS subjects as negative samples in true positive (TP), false positive (FP), true negative (TN) and false negative (FN) calculations.

We compared our OS prediction performance with that only using low-order or high-order connectomics as features. We also calculated the performance of using a simple clinical model with only 13 traditional features. Please note that the prognosis model with only 13 features may be over-simplified, which was only used as a baseline. Besides, we also adopted several other commonly adopted low-order connectomics construction methods for performance comparison. These methods are *1)* Pearson's correlation-based brain FC network construction, *2)* partial correlation-based brain FC network construction, and *3)* connectivity strength-weighted sparse representation-based brain FC network construction (Yu et al. 2016b).

Extracting the brain regions and connectivities with prognostic ability

To further identify imaging biomarkers with potential prognostic value, we identified the connectomics features with the most discriminative (prognostic) ability from both low- and high-order connectomics, if they were selected for more than 60 out of the 68 LOOCV runs. As each node in the high-order connectomics corresponds to a cluster consisting of multiple brain region pairs, we showed all the involved brain region pairs as the most discriminative high-order FC features.

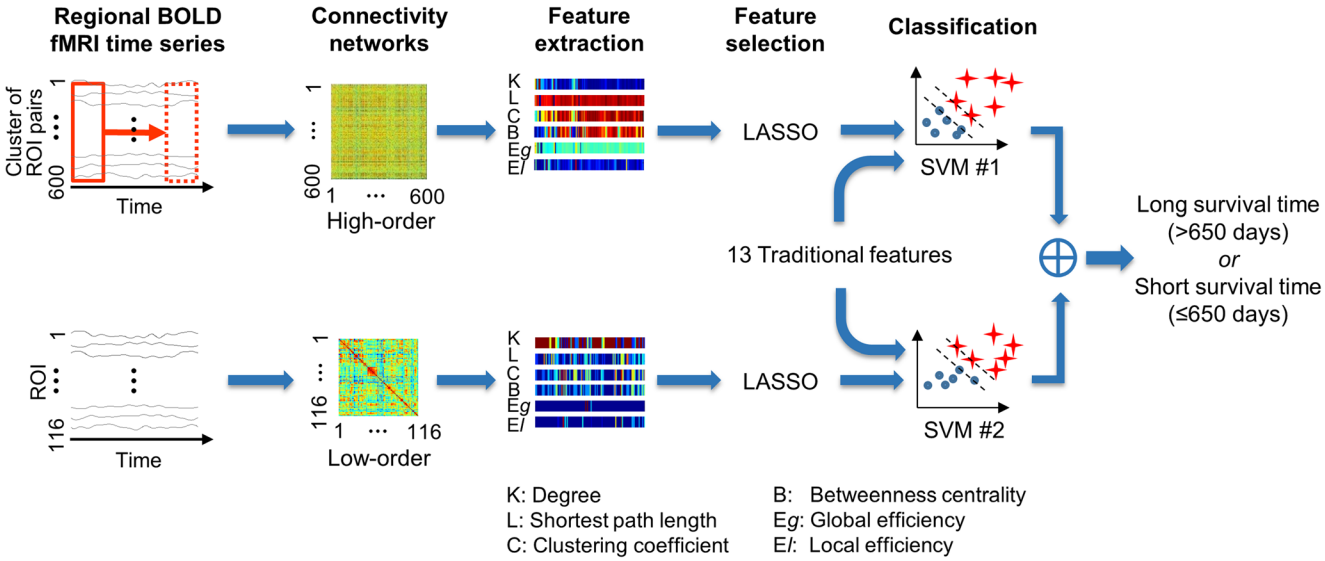

Fig. 1 Proposed pipeline of OS prediction for high-grade glioma patients. First, valuable features are effectively extracted from the low- and the high-order connectomics. Then, a simple and efficient LASSO feature selection method is performed to identify good features and reduce feature redundancy. After that, two SVMs are built based on the features selected from the low- and high-order connectomics, respectively. Finally, a decision-level fusion classification method is used to combine the classification results from two SVMs together to make full use of the information contained in static and dynamic brain functional networks. K: degree; L: shortest path length; C: clustering coefficient; B: betweenness centrality; Eg: global efficiency; and El: local efficiency

Data availability The datasets generated during and/or analyzed during the current study are not publicly available due to the institution policy of Huashan Hospital but are available from the corresponding author on reasonable request.

Results

Exemplary cases

Figure 2 shows two patients with WHO-IV gliomas (i.e., glioblastoma), both at young ages, with presurgical neurological deficits but relatively high KPS scores, received gross total resection and similar post-surgical treatments. However, these two patients have different OS. For example, subject #001 only lived less than one year, while subject #147 is still alive according to the last follow-up for three and a half years. Compared with subject #001, subject #147 had a larger glioblastoma, which could have made his/her prognosis less favorable if OS was simply associated with the presurgical tumor size. If simply evaluating OS based on the extent of resection, subject #147 could have similar OS estimation as, if not better than subject #001. As for the tumor imaging appearance, both subjects have a ring-shaped enhancement along the rim and a necrosis region in the kernel of the tumor, as well as similarly heterogeneous tumor entity and hypo-intensity edema area. Based solely on such imaging appearance, it is difficult to make prominently different prognosis prediction results for them. Of note, by using the two cases, we intended to indicate that it could be quite complicated to engineer tumor-based image appearance (radiomics) features for prognosis because of the highly heterogeneous local appearance of the tumor entity. Other features such as connectomics could also provide information for OS prediction as valuable as those previously used radiomics features, but these two types of the features are quite different from each other.

Overall survival prediction accuracy

The OS prediction accuracy of our proposed framework (utilizing both low- and high-order connectomics as well as the traditional clinical information) is significantly higher than that using only 13 clinical features (accuracy = 86.8% vs. 63.2%). Except for comparing our proposed method with the method using only clinical features and other state-of-the-art connectomics-based methods, we also compared with the methods using radiomics features. Like the previous tumor radiomics studies, we extracted higher-level image features from multimodal images (T1-weighted MRI, rs-fMRI and DWI) using the well-adopted scale-invariant transform (SIFT) and Haar-like features. Specifically, we first manually drew a bounding box that best includes the entire tumor areas according to the T1-weighted MRI. We then registered all other imaging modalities to the T1 image for each patient. For rs-fMRI, we computed amplitude of BOLD signal fluctuations at each frequency band to represent brain activities (Buzsaki and Draguhn 2004). For DWI, we computed various diffusivity metrics, such as fractional anisotropy (FA) (Alexander et al. 2011). We extracted both SIFT (Lowe 2004) and Haar-like (Viola and Jones 2004; Zhang et al.

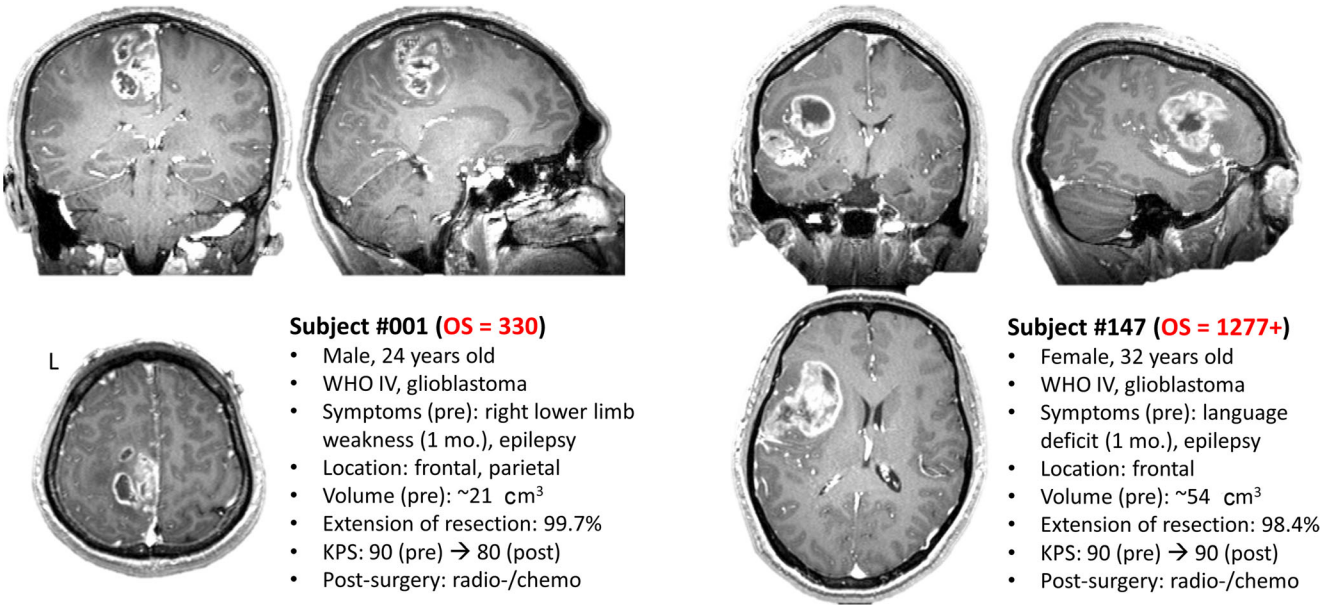

Fig. 2 Exemplar cases. T1-weighted contrast-enhanced images showing gliomas from two subjects who had similar imaging characteristics but quite different survival time

2017b) features from all the modalities and all metric maps and used principal component analysis (PCA) to reduce the feature dimensionality for training the SVM classification model. As shown in Table 2, although we used more imaging modalities, the accuracy in OS prediction based on the SIFT and Haar-like features was only 69.1 and 78.4%. The conventional low-order FC features calculated using Pearson's correlation and partial correlation resulted in worst performance, compared with that using the 13 clinical features. By using the state-of-the-art FC network construction method (i.e., weighted sparse representation), the OS prediction accuracy was increased prominently (by ~10% and ~15%, compared with those using only traditional features and Pearson's correlation, respectively). In contrast, even though only either low- or high-order connectomics features are used for prediction, the accuracy is increased to a satisfactory level (80.9 and 85.3%, respectively). Of note, the accuracy of our new method (86.8%) is significantly higher than that reported by our short conference paper with traditional network-based OS prediction (75%) (Liu et al. 2016). The ROC (receiver operating characteristic) curves of our proposed method and the competing methods are shown in Fig. 3.

Low-order connectomics features with high prognostic ability

The total number of the selected important low- and high-order connectomics features are three and 16, respectively. There are *no* traditional features consistently selected in 60 out of the 68 LOOCV runs. The three most important low-order connectomics features involve three brain regions and two network property metrics. They are the clustering coefficient of the left paracentral lobule (PCL.L), and the degrees of both the left supplementary motor area (SMA.L) and the left supramarginal gyrus (SMG.L). We further visualize them and compare their respective network property metrics between the short and long OS groups, to further reveal their differences between the two groups. We also checked the group differences for their right hemisphere counterparts. As shown in Fig. 4, the degree at the SMG. L is larger for the short OS group than the long OS group ($p < 0.001$), whereas such a difference is not statistically significant for the right SMG ($p > 0.05$). The degree at the SMA. L shows a similar

Table 2 Overall survival prediction performance when different features were utilized

Features	ACC	SEN	SPE
Traditional	63.2	61.8	64.7
Pearson's correlation (static)	58.8	55.9	61.8
Partial correlation (static)	57.4	52.9	61.8
Haar-like (radiomics)	69.1	73.5	65.8
Weighted sparse representation (WSR, static)	73.5	76.5	70.6
SIFT (radiomics)	78.4	80.0	77.3
Low-order (LO) connectomics (static)	80.9	79.4	82.4
High-order (HO) connectomics	85.3	85.3	85.3
Our method (LO + HO + Traditional)	86.8	85.3	88.2

Traditional: only using traditionally clinical information as features (see *Machine-learning-based overall survival prediction* section and Electronic Supplementary Materials for details). "Static" indicates that the feature represents static brain functional connectivity, instead of dynamic functional connectivity as used in high-order connectomics. SIFT: scale-invariant transform; ACC: accuracy; SEN: sensitivity; and SPE: specificity

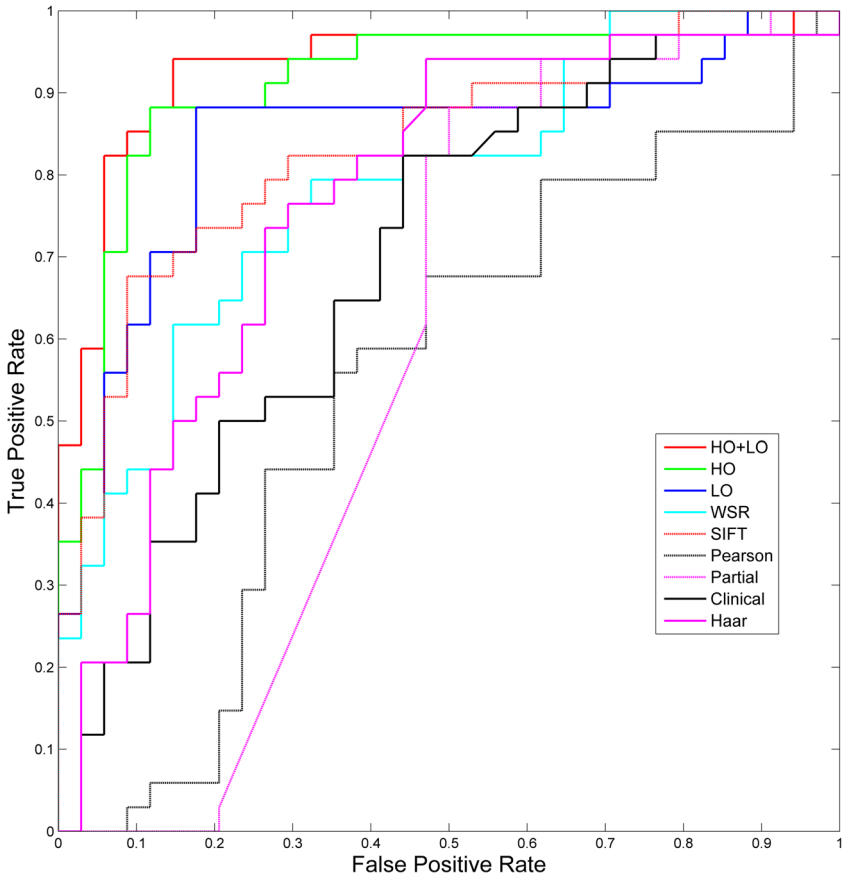

Fig. 3 The ROC (receiver operating characteristic) curves of proposed methods and the competing methods. HO: high-order; LO: low-order; WSR: weighted sparse representation; and SIFT: scale-invariant transform

result, with a significant group difference on the left side but not on the right side. For PCL. L, the short OS group still has significantly higher local clustering coefficient than the long OS group ($p < 0.001$), and its right-side counterpart shows a much weaker difference ($p < 0.05$).

High-order connectomics features with high prognostic ability

It is quite important to visualize the high-order connectomics features in an intuitive way for better understanding of the biological meaning of the high-order FC. Thus, we showed each high-order FC cluster with a spatial distribution of co-varied FC dynamics (a set of brain-region pairs). Figure 5 shows the high-order "nodes" with higher OS predictability. More details of these high-order FC clusters can be found in Electronic Supplementary Materials. Interestingly, the co-varied FC dynamics seem well organized structurally, and such structural patterns can be generally divided into two types: stars (Fig. 5a–l) and symmetric grids (Fig. 5m–p). For the star-shaped high-order FC, there is usually one (or two closely located) brain region (s) which serves as a "hub (s)" with extensive connections to other regions. While these non-hub regions usually do not interconnect with each other. In the corresponding adjacent matrix, this high-order FC corresponds to a crossing pattern, indicating a center region with a large degree. Among all the 12 star-shaped high-order FC clusters, six clusters have a single (or two) cerebellar region (s) as hub (s); two have a single (or two) subcortical region (s) as hub (s); and four have an association region (s) as hub (s). Except the two spatially symmetric high-order FC clusters centering at the vermis, all other ten high-order FC clusters have asymmetric spatial distributions.

The two high-order FC clusters with symmetric grid-like pattern involve cortico-subcortical connections (Fig. 5o, p), i.e., one involving orbitofronto-temporal connections (Fig. 5m) and the other involving cerebro-cerebellar motor pathway (Fig. 5n).

Discussions

General discussion

In this work, we demonstrate a high accuracy (86.8%) in individualized OS stratification for HGG patients using features from whole-brain FC networks based on a single-site preoperative rs-fMRI data. The prediction is conducted based purely on the presurgically obtained features. We propose that, given typical surgical and post-surgical treatments, the OS time could be roughly predicted by using presurgical rs-

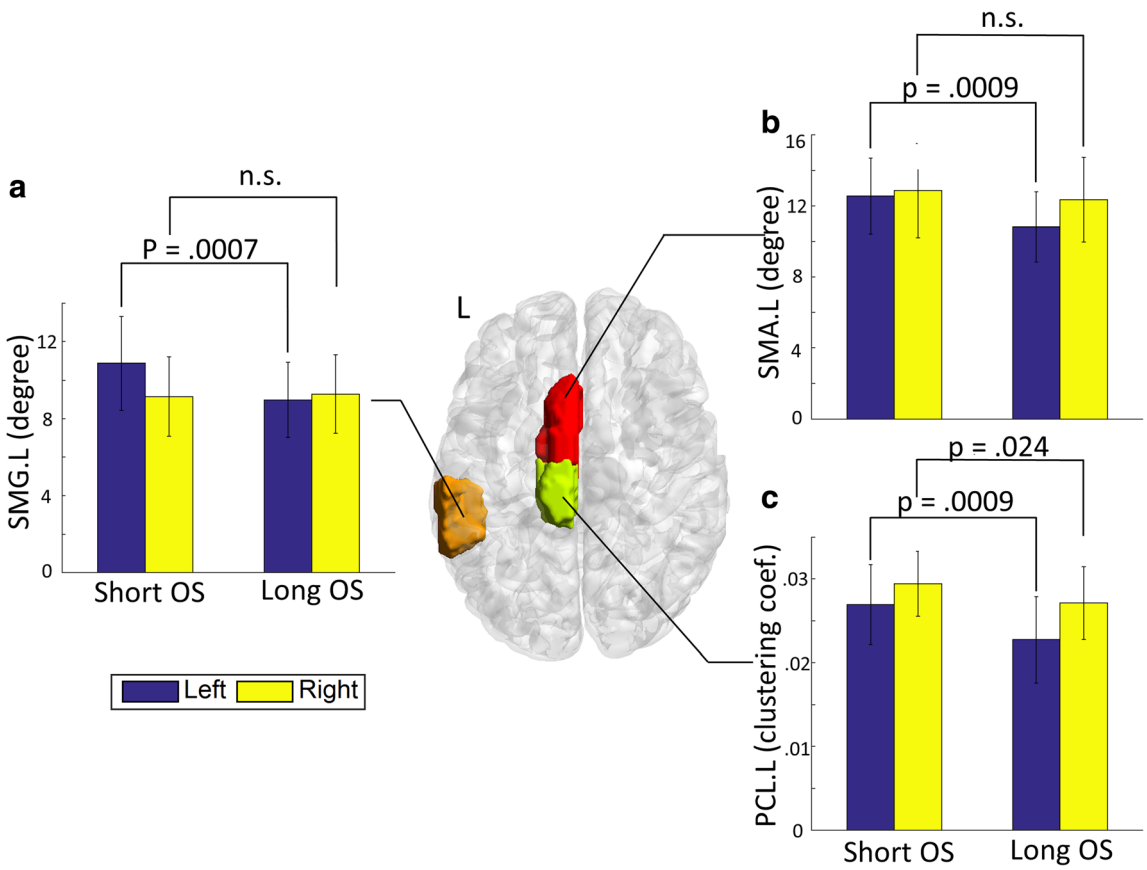

Fig. 4 Discriminative ROIs with consistent predictive ability for low-order functional connectomics. The statistical comparison results between two OS groups are provided, together with the results at their right-side counterparts. OS: overall survival time; SMG.L: left supramarginal gyrus; SMA.L: left supplementary motor area; PCL.L: left paracentral lobule; n.s.: non-significant. The figure was drawn by using BrainNet Viewer (Xia et al. 2013)

fMRI. Although it is still far away from real clinical application due to the limited sample size and the rough OS classification rather than regression, our study still indicates a promising clinical value of human brain connectomics for HGG prognosis evaluation. Most importantly, we show significant improvement in OS prediction with connectomics features compared to the traditional pre-surgical prognosis evaluation with 13 general clinical features. Our study indicates that normal-appearing brain tissues may carry essential prognostic information, which has been largely omitted previously. Such information may reflect the influence of the gliomas on the brain, intrinsically associated with patients' physical statuses, thus with the prognostic value given routine treatment. This is a great example showing how a dedicated imaging technique and post-processing analysis can contribute to the traditional clinical practices.

As a proof-of-concept study, we successfully classified the subjects with bad OS from those with good OS using a classification framework, a testbed of future regression-based OS (as a continuous variable) length prediction. Of note, as a preoperative OS prediction study, we deliberately used the subjects with matched status and treatment. We only compared the performance of our OS prediction model with a simple "traditional model" with only mostly used 13 "clinical" features. We fully acknowledge the previous works using other informative prognostic features such as molecular biomarkers (e.g., isocitrate dehydrogenase 1, or IDH1) and treatment variables (e.g., the extent of resection and the dose of radiotherapy). Our study is to provide a presurgical OS prediction with brain images to guide the clinical intervention, rather than that based on the exhaustively collected features, which is time-consuming and unrealistic. We acknowledge that molecular and genomic biomarkers could also predict OS (Cairncross et al. 1998), but they can only be obtained in an invasive way. We also believe that clinical intervention and recovery nursing care can largely affect OS. Therefore, the main advantage of our model is that we have proved that the prognostic features can be extracted from presurgical non-invasive brain functional imaging.

Traditional or imaging-based prognostic evaluation

For HGG patients, comprehensive presurgical assessment is essential in clinical practice. In addition to the tumor

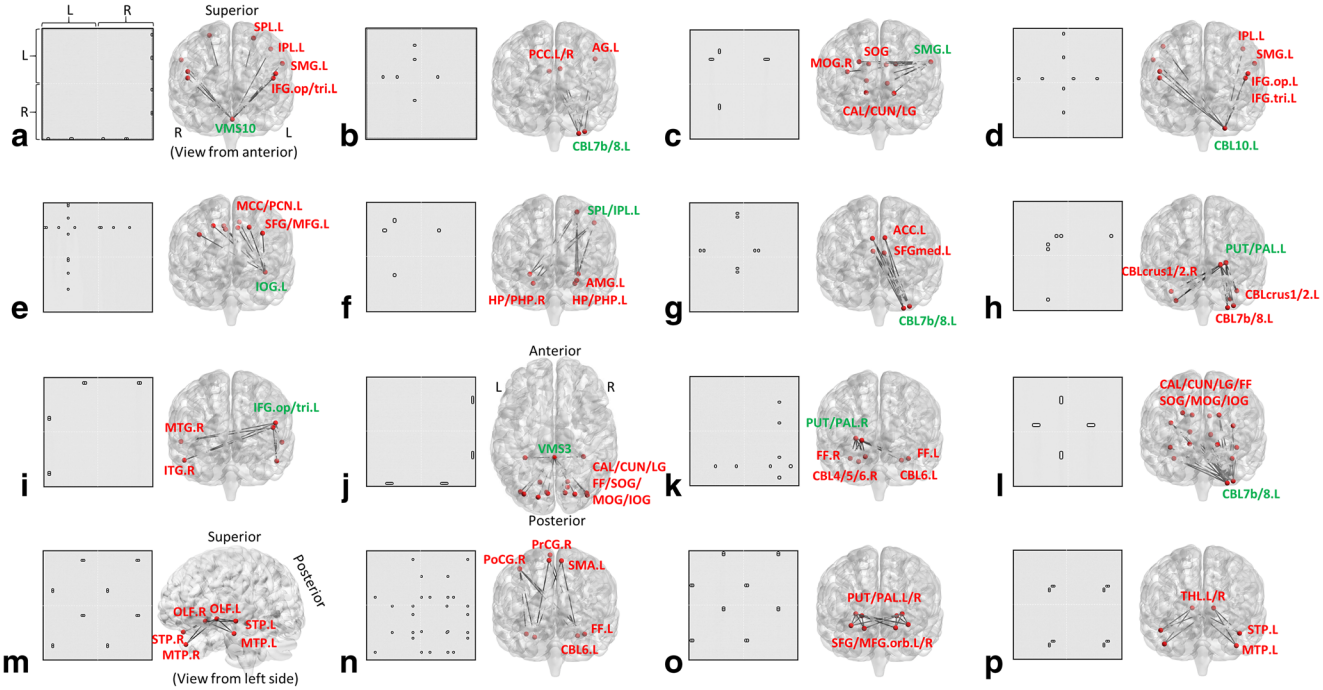

Fig. 5 Discriminative high-order FC patterns with consistent predictive ability. A total of 16 "hyper-nodes" in the high-order networks where the nodal properties could consistently predict OS were shown. In each of the subplots (**a-p**), a spatial pattern corresponding to a set of pairwise dynamic FC links was shown, both with an adjacent matrix (with re-organized column and row orders, with the first and second halves of the adjacent matrix representing the left and right hemispheres, respectively) and a brain volumetric rendering result (based on BrainNet Viewer, www.nitrc.org/projects/bnv). Each set of dynamic FC links has similar temporal fluctuation patterns; as a result, they were grouped together based on clustering and the center of the cluster was further used for high-order FC calculation. Therefore, each of the subplots was treated as a hyper-node of the high-order FC networks. Each element of the adjacency matrices represent a different pairwise link, and each cluster has multiple such pairwise links. From 12 (subplots **a-l**) out of 16 hyper-nodes, "hub-peripheral" patterns were identified, with the "hub" regions shown in green, and other peripheral regions which connected to the hubs shown in red. From the remained 4 hyper-nodes (subplots **m-p**), symmetric patterns were found, with symmetric bi-hemispheric links involved. For multi-view version of this figure and the fullnames of the brain regions, please see Electronic Supplementary Materials

localization and eloquent functional area localization (if the tumor is located in the proximity of the functional areas, such as sensorimotor and language areas), prognostic evaluation has been usually, if not explicitly, conducted by the doctors to better assist treatment. However, the multidiscipline barriers among radiodiagnosticians, imaging technicians, radio/chemotherapists, pathologists, neuro-oncologists and neurosurgeons pose a great challenge to this practice. Insufficient information, a misunderstanding during the information exchange, or different criteria used by different physicians could make prognostic evaluation difficult. Traditionally, several descriptive features from demographics (e.g., age) or physical status data (e.g., KPS) or the tumor histopathology (obtained by either expert evaluation of the clinical images or biopsy specimen) have been widely used to evaluate the OS roughly. However, clinically accurate and sensitive prognostic indicators are still not apparent, making individualized prognostic evaluation infeasible (Davis et al. 1998). This can be indicated by our result using only 13 traditional features with an accuracy of 63.2%. The reasons for the unsatisfactory accuracy in the "traditional feature"-based OS prediction could be the highly heterogeneous tumors characteristics across patients, too complex interaction among these factors, and/or ignoring other hidden factors. Neuroimaging techniques can non-invasively reveal the brain phenotype information, from which one can identify abundant prognostic information. Therefore, imaging phenotype-based prognosis has gained increasing interests. In future, phenotype and genotype data should be jointly used for OS prediction in routine clinical practice.

We think that simple behavioral and physical examine scales (such as KPS) cannot provide adequate sensitivity for individualized OS prediction. For example, in our study, preoperative KPS for all the tumor patients are larger than 80 (with most of them being larger than 90), leading no significant difference between the two OS groups ($p > 0.99$). Such inadequate sensitivity also exists for most of the traditional features (e.g., tumor size and location). Previously, studies comparing KPS scores between glioma patients and healthy controls found a significant group difference (Jain et al. 2014; Klein et al. 2001); however, when both groups have tumors but with different OS, there may be no difference in KPS. We propose that more sensitive features should be used for OS prediction in future to comprehensively measure physical,

cognitive, affective and psychological statuses. This is because that the differences between short and long OS groups could be subtle, with probably slightly more complaints of occasional cognitive disturbances, fatigue and mood disorders for the patients with short OS (Taphoorn et al. 1994). FC could be more sensitive to such subtle changes, which has been supported by many previous studies on the brain disease detection at a prodromal stage (Zhang et al. 2016; Chen et al. 2016a).

As shown by the tumor probability maps (Electronic Supplementary Materials), the tumors of the two groups in our study seem to be similarly located at the left insula and its nearby regions. Please note that, while statistical analysis on tumor location did not show significant group difference, we still could not claim that tumor location is irrelevant to the OS, as several studies have suggested that different tumor locations could indicate different prognosis (Jeremic et al. 1994; Simpson et al. 1993). We think that, similar lesion location between the two groups in our study could still lead to global differences in the connectomics, and that the latter could be more relevant to survival time. This leads to the following discussion and comparison of the prognostic values between global connectomics and local radiomics.

Prognostic values of brain connectomics and radiomics

Based on the presurgical images, there are two main strategies to extract features for OS prediction: connectomics- and radiomics-based methods. In this paper, we adopted the former, while all the previous OS prediction studies have adopted the latter. Aside from the aforementioned advantages of the connectomics compared to the radiomics, here we deeply analyze the potential biological mechanisms that lead to the success of connectomics-based OS prediction. First, we hypothesized that prognosis is not only related to treatment but also closely associated with presurgical healthy status as reflected by the connectomics. This is supported by many studies showing the association between OS (or recurrence and severity) and patients' life quality, physical status and neurobehavioral/cognitive status (Martin Klein et al. 2001; Taphoorn et al. 1994; Giovagnoli et al. 2005). However, most studies aimed at investigating how treatment affects the neurological, cognitive and psychological abilities in the postsurgical studies (Klein et al. 2002). We think that the presurgical assessment of these functions is also equally crucial for OS assessment. FC has long been applied for the early detection of various brain diseases, such as Alzheimer's disease (Stam et al. 2007) and schizophrenia (Lynall et al. 2010). In addition, altered connectomics have also been linked to abnormal cognitive and behavioral statuses (Sporns et al. 2004). Therefore, the connectomics might be used to evaluate healthy statuses and predict OS for the HGG patients (Maesawa et al. 2015).

Second, differences in brain functional connectomics may reflect the stage of the gliomas. We originally hypothesized that severer tumor (with shorter OS) could cause larger direct and indirect interferences to the brain connectomics. However, we found that the network property metrics on the tumor side have much higher values compared to those on the contralateral side (Fig. 4). This leads to a different interpretation to the tumor-induced connectomics alterations. That is, at the beginning of the glioma growth, the tumor can be regarded as a local pathological interference that could make a *direct*, *local* disturbance to the brain connectomics. For example, Agarwal et al. (2017) found that local FC was reduced in the tumor regions. While a tumor is growing, penetrating, and taking places with more surrounding brain tissues, its influence on the brain connectomics could widely spread. The brain may evolve and adapt to the neoplasm, leading to other *indirect*, *plastic* changes at "normal appearing" regions or even on the unaffected side (Hart et al. 2016a; Maesawa et al. 2015; Ghumman et al. 2016; Wang et al. 2010). Hart et al. (2016b) suggested that different tumor locations might affect different functional networks. They further found significant FC network alterations in the glioma patients compared with healthy controls (Hart et al. 2016a). In our study, we step further and found differences in the FC network properties even within the brain tumor cohort between long- and short-OS groups. In contrast, radiomics features mainly focus on local appearance changes, thus may ignore a significant amount of systemic prognostic information or include nuisance features that may only reflect lesion-related but no OS-associated appearance changes. This has been further proved by our additional experiments extracting state-of-the-art radiomics features from the same data for the OS prediction, including scale-invariant transformation (SIFT) (Lowe 2004), and Haar-like features (Viola and Jones 2004), with the accuracy of 78.4 and 69.1%, respectively (Table 2).

Third, compared to the radiomics features that could be more affected by the tumor heterogeneity, connectomics features measure systemic and global changes, which might be less affected by such a heterogeneity. In addition, the reliability and robustness in feature extraction are important to successful OS prediction. These are supported by the inferior performance (accuracy = ~50%) using traditional brain network construction methods (Pearson's/partial correlation) compared with the more robust methods (weighted sparse representation and our robust low-order connectomics construction, with ~70–80% in accuracy). Specifically, Pearson's/partial correlation-based methods could be more vulnerable to the tumor interference and less robust to noise and artifacts. The sparse representation-based methods, however, are able to suppress noise (Yu et al. 2016b). Moreover, these methods can characterize more complex interactions among multiple brain regions (Meinshausen and Bühlmann 2006) to provide more sensitive features for OS prediction.

The difference between our low-order FC network construction method and weighted sparse representation is that we not only use FC strength as a weight to suppress noise and construct biologically meaningful networks but also explicitly use a robust representation term in the cost function to further suppress noise.

With significantly increased prognosis accuracy, we can further analyze which features could contribute to the OS prediction and why. Since low- and high-order FC was separately calculated and jointly used for OS prediction, the important prognostic features for these two types of connectomics could be fundamentally different, which will be separately discussed below.

The most predictive low-order FC features

Based on the involved neurological functions and the locations relative to the lesion probability map, we attribute the selected predictive low-order FC (Fig. 4) as a consequence of the lesions. The involved regions are located at either language or sensorimotor-related areas, all in the left hemisphere, same as the hemisphere with high tumor probability. This can explain why most of the subjects have deficits in language and/or motor functions. Among them, the supramarginal gyrus is mainly related to language perception and receptive processing (Gazzaniga 2009). It is also believed to be part of the somatosensory association cortex that mediates perception of space and limb location, as well as identifying postures and gestures of other people (Carlson 2010). This region works closely with the surrounding areas, such as the angular gyrus, to integrate complex signals sent from other primary and secondary regions. The other two regions are both related to sensorimotor function, including motor planning, making sequences of movement, and motion coordination (He et al. 1995) for the left supplementary motor area, as well as controlling motor/sensory innervations of the lower extremity for the left paracentral lobule.

We further investigated how such influences differed between two OS groups. For the two left-side sensorimotor-related regions, interestingly, short OS group has a larger degree/clustering coefficient than the long OS group (Fig. 4b, c). For the language related region, such a group difference still holds for the left-side region, but not the right-side counterpart (Fig. 4a). The right-side regions were served as internal controls, where no significant group difference was found (except a weak group difference on the clustering coefficient at the right paracentral lobule). Such findings indicate that, although these three regions could be directly affected by tumors, they may not be the direct cause of OS differences. Next, we provide two hypotheses to interpret these findings.

First, the cost to compensate for tumor influence on the connectomics could be higher in the short OS than the long OS group. The increased degree and increased clustering coefficient could be associated with abnormally increased network local efficiency due to the adaptive mechanism to the local disturbance to the network caused by the nearby neoplasms. Due to the effect of tumors, the brain has to increase the FC in the adjacent areas of the lesions to take over the dysfunctional regions to maintain the normal functions. Such an abnormally increased connection burden can affect a node itself by increasing its degree or influence its neighboring connections by increasing its clustering coefficient. Similarly, Carbo et al. (2017) also found with magnetoencephalography (MEG) that patients with different brain tumors have over-loaded hubs that are negatively correlated with their presurgical cognitive ability (i.e., the higher the nodal degree is, the lower the executive and attentional performance will be). In a longitudinal study on the efficiency change of the sensorimotor network during stroke recovery, Wang et al. (2015b) found that, the network could shift toward a random and less efficient network with increased degrees. Moreover, Yu et al. (2016a) found differences in network hub location between brain tumor patients and healthy controls. Our findings may provide additional support to such a compensatory hypothesis.

The second possible interpretation is that the plastic network reorganization could be more significant in the long OS group due to the slower tumor growth than the short OS group. A shorter OS may correspond to faster-growing HGG, and vice versa. This could be supported by the previous studies comparing low-grade gliomas with HGGs. It is believed that low-grade gliomas have a slower growth rate (Duffau 2017; Stensjøen et al. 2015), making the brain functional reorganization have enough time to take place (van Dellen et al. 2012; Desmurget et al. 2007), thus resulting in more prominent network reorganization. In contrast, HGGs are generally faster growing, leaving little time for the brain connectomics to reshape or reorganize (Aerts et al. 2016; van Dellen et al. 2012). The difference in the tumor growth rate does not only exist between low-grade and high-grade gliomas, but also between different subjects with HGGs. Stensjøen et al. (2015) found that the tumor growth for the HGGs could vary largely across subjects, even for those with the same WHO grade. This could explain our findings in the sensorimotor network (Fig. 4b, c), where the degree on the lesion side of the sensorimotor area in the short OS group is similar ($p = 0.58$, paired t-test) to that on the contralateral side of the sensorimotor area, while the long OS group shows significantly different degree between the left and right sensorimotor areas ($p = 0.002$). A similar trend can also be found based on the clustering coefficient at the left paracentral lobule, another region in the sensorimotor network.

Of note, several previous empirical studies on brain tumor patients found inconsistent results regarding to the brain

network changes (Aerts et al. 2016; Bartolomei et al. 2006; Bosma et al. 2009; van Dellen et al. 2014; Huang et al. 2014; H. Wang et al. 2010; Xu et al. 2013). For example, Xu et al. (2013) and Yu et al. (2016a) found no group difference in the global clustering coefficient of the whole connectomics between low- and high-grade gliomas. This could be due to the fact that the global network properties used in these studies are not sensitive to the local tumor lesion. In contrast, we investigated nodal properties (i.e., degree and local clustering coefficient) and found significant changes that are associated with different OS. Moreover, compared to the sample size of the previous studies as reviewed by Aerts et al. (2016), our sample size is larger ($N = 68$) compare to $N = 34$ in Yu et al. (2016a). Meanwhile, our patients are more homogenous (all HGG patients) compare to three meningiomas, seven low-grade gliomas and seven HGGs used in (Yu et al. 2016a).

The most predictive high-order FC

There are 16 high-order connectomics features selected as robustly predictive features (Fig. 5 and Electronic Supplementary Materials), which are more than the selected predictive low-order connectomics features. Such an increase in predictive features could be due to the fact that high-order FC measures higher level and more complex brain functional associations and could be more sensitive to OS differences compared to low-order FC (Chen et al. 2016a, b; Zhang et al. 2017a). In this study, each high-order hyper-node may contain more than two dynamic connections due to the clustering analysis we used to reduce network dimension. Due to the complexity of these high-order hyper-nodes, we visualized each of them using a brain network plot that shows all the involved dynamic connections in each cluster, without further interpreting the hyper-edges or high-level network properties.

We found two interesting structured patterns for the 16 most informative high-order FC features. The first type is star-shaped high-order FC clusters, with one (or two) region (s) at the center (s) and all others at the peripheral without direct links to each other. Such a pattern may indicate that the central region acts as a driving region while all the peripheral regions are driven by it. In such a pattern, the driving central region could dominate the entire high-order FC cluster, making itself act as a hub. We note that most of the driving regions are located in the cerebellar regions, with most of the peripheral regions are distributed symmetrically in the cortical areas. We further focused only on the representative link nearest to the high-order FC cluster center and drew them in Electronic Supplementary Materials. We found a dominant pattern from the result that involves dynamic FC connecting the cerebral cortex and the cerebellar areas. The findings provide further evidence of the important OS-related functions mediated by the cerebro-cerebellar connections. The cerebellum has been considered to mediate motion coordination and synchronization. It also connects with many cortical regions and is responsible to regulation and modulation of attention, language, memory, emotion, and other high-level cognitive functions (Ratey 2001; Squire et al. 2012). By using high-order FC, we found that most of the cortical nodes in the most predictive cerebro-cerebellar connections are distributed into multiple high-order functional systems, such as the frontal-parietal task control network (Fig. 5a, d), default mode network (Fig. 5b, g) and visual network (Fig. 5j, l). Therefore, we think that the high-order function-related cerebro-cerebellar connections can predict OS. Beside the cerebellar regions, other driving hubs mostly involve the high-level association areas, such as supramarginal gyrus, inferior occipital gyrus, superior/inferior parietal lobules, inferior frontal gyrus, and striatum. This further demonstrates the ability of high-order FC in capturing high-level complex brain functions.

Similarly, previous studies on the FC dynamics also found a similar star-shaped pattern. Using rat model, Grandjean et al. (2017) found that one of the brain dynamic statuses also formed a star shape, with the thalamus as a central region and all other cortical regions as peripheral regions (see the dynamic functional status #16 in Fig. 3 of Grandjean et al. 2017). There is no further interpretation of this star-shaped status, but they tentatively linked it with chronic psychosocial stress, a negative emotional state). Gu et al. (2017) also reported a star-shaped hyper-edge during the investigation of different types of FC hypergraphs defined by the correlation between any pair of the static low-order FC links across subjects. They further proposed that the star-shaped hyper-edges constitute dominant and fundamental motifs in the brain, which may be involved in information integration processes from diverse sources to a single brain region or in an information broadcasting processes from a single region to distributed nodes. Our findings provide another possible interpretation of this type of high-order FC clusters by linking it to the OS prediction. We propose that the star-shaped high-order FCs might be related to high-level cognitive and emotional statuses that have a prognostic value. We further suggest that those statuses are pivotal to physical and mental health that are highly associated with prognosis.

A second type of the high-order FC clusters is symmetric inter-hemispheric connectivity grid (Fig. 5m–p), where each region is involved in a cross-hemisphere connection linking with its mirrored counterpart. Among the four high-order FC clusters, two are the cortico-subcortical high-order FCs involving both striatum and thalamic regions, as well as the orbital frontal regions and temporal pole; a third cluster has a spatial pattern involving the interactions between the orbital frontal regions and temporal pole, and the last cluster covers the sensorimotor system. There is no dominant hub nor driving region in them. We hypothesize that such a pattern reflects interhemispheric coordination that may be affected by the

tumors. The orbitofrontal regions are related to social cognition, reward-related emotional processes and decision making (Fuster 1988). The connections between the orbitofrontal regions to temporal pole, thalamus and striatum may be responsible for inhibitory and excitatory regulations of the autonomic function (Cavada et al. 2000), goal-directed and habitual action (Balleine and O'doherty 2010), as well as visual/auditory information association and integration (Cavada et al. 2000). The temporal pole is also related to social and emotional processes (Olson et al. 2007). Collectively, this type of high-order FC clusters could also mediate high-level cognitive and emotional functions, which could be affected by the HGGs.

Limitations

There are several limitations in this study. First, the limited sample size could lead to a concern about model generalizability. In routine clinical practice, not every patient has a rs-fMRI scan for calculating the functional connectomics. Moreover, OS calculation requires a long follow-up period, which further limits the available sample size. With a larger sample size, one can conduct a regression analysis rather than the two-class (short vs. long OS) classification as used in the current study, for better and more realistic OS prediction. Second, due to the retrospective type of this study, most of the included subjects have tumors near the language and motor areas. It leads to a left dominant tumor distribution pattern. In the future, a prospective, well-designed study that can balance the tumor distribution between both hemispheres should be conducted. Third, the traditional clinical information used in this study was not exhaustively explored. A comprehensive feature extraction could further increase OS prediction accuracy. An ongoing study by us is to use deep-learning-based features (Nie et al. 2016), connectomics features, and genomic features to jointly predict the OS. Finally, we only demonstrated the feasibility of the presurgical OS prediction. The OS should be also related to other treatment-related variables, and the OS prediction should be gradually updated based on longitudinal data.

Conclusions

This is the first successful implementation of individualized overall survival time prediction for brain tumor patients based on presurgical non-invasive brain functional imaging and following whole-brain large-scale network analysis. We proposed novel techniques to calculate different types of functional connectomics to extract robust and comprehensive features for outcome prediction. With all connectomics features, we achieved 86.8% accuracy, which is a significant improvement compared with prognosis based on traditional clinical and demographic information. The results show a good feasibility of preoperatively predicting overall survival time under the condition of total resection and clinical routine post-surgery treatment for high-grade gliomas. Our study also indicates a promising direction for human brain connectomics applications to individualized prognosis in precision medicine.

Acknowledgments This work is partially supported by National Natural Science Foundation of China (NSFC) Grants (61473190, 61401271, 81471733, 81201156, and 81401395), the National Key Technology R&D Program of China (2014BAI04B05), and NIH grant (EB022880).

Compliance with ethical standards

Disclosure The authors report no conflict of interest concerning the materials or methods used in this study or the findings specified in this paper.

Ethical approval All procedures performed in studies involving human participants were in accordance with the ethical standards of the Huashan Institutional Review Board and with the 1964 Helsinki declaration and its later amendments or comparable ethical standards.

Informed consent Informed consent was obtained from all individual participants included in the study.

References

Aerts, H., Fias, W., Caeyenberghs, K., & Marinazzo, D. (2016). Brain networks under attack: Robustness properties and the impact of lesions. *Brain, 139*(12), 3063–3083.

Agarwal, S., Sair, H. I., & Pillai, J. J. (2017). The resting state fMRI regional homogeneity (ReHo) metrics KCC-ReHo & Cohe-ReHo are valid indicators of tumor-related neurovascular uncoupling. *Brain Connectivity, 7*(4), 228–235.

Aibaidula, A., Lu, J.-F., Wu, J.-S., Zou, H.-J., Chen, H., Wang, Y.-Q., et al. (2015). Establishment and maintenance of a standardized glioma tissue bank: Huashan experience. *Cell and Tissue Banking, 16*(2), 271–281.

Alakorkko, T., Saarimaki, H., Glerean, E., Saramaki, J., & Korhonen, O. (2017). Effects of spatial smoothing on functional brain networks. *The European Journal of Neuroscience, 46*, 2471–2480.

Alexander, A. L., Hurley, S. A., Samsonoy, A. A., Adluru, N., Hosseinbor, A. P., Mossahebi, P., et al. (2011). Characterization of cerebral white matter properties using quantitative magnetic resonance imaging stains. *Brain Connectivity, 1*, 423–446.

Ashburner, J. (2007). A fast diffeomorphic image registration algorithm. *Neuroimage, 38*(1), 95–113.

Ashburner, J., & Friston, K. J. (2005). Unified segmentation. *NeuroImage, 26*(3), 839–851.

Balleine, B. W., & O'doherty, J. P. (2010). Human and rodent homologies in action control: Corticostriatal determinants of goal-directed and habitual action. *Neuropsychopharmacology, 35*(1), 48–69.

Bartolomei, F., Bosma, I., Klein, M., Baayen, J. C., Reijneveld, J. C., Postma, T. J., et al. (2006). Disturbed functional connectivity in brain tumour patients: Evaluation by graph analysis of synchronization matrices. *Clinical Neurophysiology, 117*(9), 2039–2049.

Bisdas, S., Kirkpatrick, M., Giglio, P., Welsh, C., Spampinato, M., & Rumboldt, Z. (2009). Cerebral blood volume measurements by

perfusion-weighted MR imaging in gliomas: Ready for prime time in predicting short-term outcome and recurrent disease? *American Journal of Neuroradiology, 30*(4), 681–688.

Biswal, B., Zerrin Yetkin, F., Haughton, V. M., & Hyde, J. S. (1995). Functional connectivity in the motor cortex of resting human brain using echo-planar MRI. *Magnetic Resonance in Medicine, 34*(4), 537–541.

Bosma, I., Reijneveld, J. C., Klein, M., Douw, L., Van Dijk, B. W., Heimans, J. J., et al. (2009). Disturbed functional brain networks and neurocognitive function in low-grade glioma patients: A graph theoretical analysis of resting-state MEG. *Nonlinear Biomedical Physics, 3*(1), 9.

Bullmore, E., & Sporns, O. (2009). Complex brain networks: Graph theoretical analysis of structural and functional systems. *Nature Reviews Neuroscience, 10*(3), 186–198.

Buzsaki, G., & Draguhn, A. (2004). Neuronal oscillations in cortical networks. *Science, 304*, 1926–1929.

Cairncross, J. G., Ueki, K., Zlatescu, M. C., Lisle, D. K., Finkelstein, D. M., Hammond, R. R., et al. (1998). Specific genetic predictors of chemotherapeutic response and survival in patients with anaplastic oligodendrogliomas. *Journal of the National Cancer Institute, 90*(19), 1473–1479.

Carbo, E. W., Hillebrand, A., Van Dellen, E., Tewarie, P., de Witt Hamer, P. C., Baayen, J. C., et al. (2017). Dynamic hub load predicts cognitive decline after resective neurosurgery. *Scientific Reports, 7*, 42117.

Carlson, N. R. (2010). Physiology of behavior. *Allyn & Bacon Boston*.

Cavada, C., Tejedor, J., Cruz-Rizzolo, R. J., & Reinoso-Suárez, F. (2000). The anatomical connections of the macaque monkey orbitofrontal cortex. A review. *Cereb Cortex, 10*(3), 220–242.

Chen, W., Delaloye, S., Silverman, D. H., Geist, C., Czernin, J., Sayre, J., et al. (2007). Predicting treatment response of malignant gliomas to bevacizumab and irinotecan by imaging proliferation with [18F] fluorothymidine positron emission tomography: A pilot study. *Journal of Clinical Oncology, 25*(30), 4714–4721.

Chen, X., Zhang, H., Gao, Y., Wee, C. Y., Li, G., & Shen, D. (2016a). High-order resting-state functional connectivity network for MCI classification. *Human Brain Mapping, 37*(9), 3282–3296.

Chen, X., Zhang, H., & Shen, D. (2016b) Ensemble hierarchical high-order functional connectivity networks for MCI classification. In *International Conference on Medical Image Computing and Computer-Assisted Intervention,* 18-25.

Chen, X., Zhang, H., Lee, S.-W., & Shen, D. (2017). Hierarchical high-order functional connectivity networks and selective feature fusion for MCI classification. *Neuroinformatics, 15*(3), 271–284.

Cochereau, J., Deverdun, J., Herbet, G., Charroud, C., Boyer, A., Moritz-Gasser, S., et al. (2016). Comparison between resting state fMRI networks and responsive cortical stimulations in glioma patients. *Human Brain Mapping, 37*(11), 3721–3732.

Collet, S., Valable, S., Constans, J., Lechapt-Zalcman, E., Roussel, S., Delcroix, N., et al. (2015). [18 F]-fluoro-l-thymidine PET and advanced MRI for preoperative grading of gliomas. *NeuroImage: Clinical, 8*, 448–454.

Cortes, C., & Vapnik, V. (1995). Support-vector networks. *Machine Learning, 20*(3), 273–297.

Cui, Y., Tha, K. K., Terasaka, S., Yamaguchi, S., Wang, J., Kudo, K., et al. (2015). Prognostic imaging biomarkers in glioblastoma: Development and independent validation on the basis of multiregion and quantitative analysis of MR images. *Radiology, 278*(2), 546–553.

Damaraju, E., Allen, E., Belger, A., Ford, J., McEwen, S., Mathalon, D., et al. (2014). Dynamic functional connectivity analysis reveals transient states of dysconnectivity in schizophrenia. *NeuroImage: Clinical, 5*, 298–308.

Davis, F. G., Freels, S., Grutsch, J., Barlas, S., & Brem, S. (1998). Survival rates in patients with primary malignant brain tumors stratified by patient age and tumor histological type: An analysis based on surveillance, epidemiology, and end results (SEER) data, 1973–1991. *Journal of Neurosurgery, 88*(1), 1–10.

Desmurget, M., Bonnetblanc, F., & Duffau, H. (2007). Contrasting acute and slow-growing lesions: A new door to brain plasticity. *Brain, 130*(4), 898–914.

Duffau, H. (2017). A two-level model of interindividual anatomo-functional variability of the brain and its implications for neurosurgery. *Cortex, 86*, 303–313.

Fan, Y., Gur, R. E., Gur, R. C., Wu, X., Shen, D., Calkins, M. E., & Davatzikos, C. (2008). Unaffected family members and schizophrenia patients share brain structure patterns: A high-dimensional pattern classification study. *Biological Psychiatry, 63*(1), 118–124.

Fornito, A., Zalesky, A., & Bullmore, E. T. (2010). Network scaling effects in graph analytic studies of human resting-state FMRI data. *Frontiers in Systems Neuroscience, 4*, 22.

Fox, M. D., & Greicius, M. (2010). Clinical applications of resting state functional connectivity. *Frontiers in Systems Neuroscience, 4*, 19.

Fuster, J. M. (1988). Prefrontal cortex. In *Comparative Neuroscience and Neurobiology* (pp. 107-109): Springer.

Gazzaniga, M. S. (2009). *The cognitive neurosciences IV.* Cambridge: MA.

Ghumman, S., Fortin, D., Noel-Lamy, M., Cunnane, S., & Whittingstall, K. (2016). Exploratory study of the effect of brain tumors on the default mode network. *Journal of Neuro-Oncology, 128*(3), 437–444.

Gillies, R. J., Kinahan, P. E., & Hricak, H. (2015). Radiomics: Images are more than pictures, they are data. *Radiology, 278*(2), 563–577.

Giovagnoli, A., Silvani, A., Colombo, E., & Boiardi, A. (2005). Facets and determinants of quality of life in patients with recurrent high grade glioma. *Journal of Neurology, Neurosurgery & Psychiatry, 76*(4), 562–568.

Glasser, M. F., Smith, S. M., Marcus, D. S., Andersson, J. L., Auerbach, E. J., Behrens, T. E., et al. (2016). The human connectome project's neuroimaging approach. *Nature Neuroscience, 19*(9), 1175–1187.

Gordon, E. M., Laumann, T. O., Adeyemo, B., Huckins, J. F., Kelley, W. M., & Petersen, S. E. (2016). Generation and evaluation of a cortical area Parcellation from resting-state correlations. *Cerebral Cortex, 26*, 288–303.

Grabner, G., Kiesel, B., Wöhrer, A., Millesi, M., Wurzer, A., Göd, S., et al. (2016). Local image variance of 7 tesla SWI is a new technique for preoperative characterization of diffusely infiltrating gliomas: Correlation with tumour grade and IDH1 mutational status. *European Radiology, 27*(4), 1556–1567.

Grandjean, J., Preti, M. G., Bolton, T. A., Buerge, M., Seifritz, E., Pryce, C. R., et al. (2017). Dynamic reorganization of intrinsic functional networks in the mouse brain. *NeuroImage, 152*, 497–508.

Grossman, S. A., Ye, X., Piantadosi, S., Desideri, S., Nabors, L. B., Rosenfeld, M., et al. (2010). Survival of patients with newly diagnosed glioblastoma treated with radiation and temozolomide in research studies in the United States. *Clinical Cancer Research, 16*(8), 2443–2449.

Gu, S., Yang, M., Medaglia, J. D., Gur, R. C., Gur, R. E., Satterthwaite, T. D., et al. (2017). Functional hypergraph uncovers novel covariant structures over neurodevelopment. *Human Brain Mapping, 38*(8), 3823–3835.

Hart, M. G., Price, S. J., & Suckling, J. (2016a). Connectome analysis for pre-operative brain mapping in neurosurgery. *British Journal of Neurosurgery, 30*(5), 506–517.

Hart, M. G., Price, S. J., & Suckling, J. (2016b). Functional connectivity networks for preoperative brain mapping in neurosurgery. *Journal of Neurosurgery*, 1–10.

He, S.-Q., Dum, R. P., & Strick, P. (1995). Topographic organization of corticospinal projections from the frontal lobe: Motor areas on the medial surface of the hemisphere. *Journal of Neuroscience, 15*(5), 3284–3306.

Horwitz, B. (2003). The elusive concept of brain connectivity. *NeuroImage, 19*(2), 466–470.

Horwitz, B., Grady, C. L., Schlageter, N., Duara, R., & Rapoport, S. (1987). Intercorrelations of regional cerebral glucose metabolic rates in Alzheimer's disease. *Brain Research, 407*(2), 294–306.

Huang, Q., Zhang, R., Hu, X., Ding, S., Qian, J., Lei, T., et al. (2014). Disturbed small-world networks and neurocognitive function in frontal lobe low-grade glioma patients. *PLoS One, 9*(4), e94095.

Hutchison, R. M., Womelsdorf, T., Allen, E. A., Bandettini, P. A., Calhoun, V. D., Corbetta, M., et al. (2013). Dynamic functional connectivity: Promise, issues, and interpretations. *NeuroImage, 80*, 360–378.

Itakura, H., Achrol, A. S., Mitchell, L. A., Loya, J. J., Liu, T., Westbroek, E. M., et al. (2015). Magnetic resonance image features identify glioblastoma phenotypic subtypes with distinct molecular pathway activities. *Science Translational Medicine, 7*(303), 138.

Jain, R., Poisson, L. M., Gutman, D., Scarpace, L., Hwang, S. N., Holder, C. A., et al. (2014). Outcome prediction in patients with glioblastoma by using imaging, clinical, and genomic biomarkers: Focus on the nonenhancing component of the tumor. *Radiology, 272*(2), 484–493.

Jeremic, B., Grujicis, D., Antunovic, V., Djuric, L., et al. (1994). Influence of extent of surgery and tumor location on treatment outcome of patients with glioblastoma multiforme treated combined modality approach. *Journal of Neuro-Oncology, 21*(2), 177–185.

Kickingereder, P., Bonekamp, D., Nowosielski, M., Kratz, A., Sill, M., Burth, S., et al. (2016a). Radiogenomics of glioblastoma: Machine learning–based classification of molecular characteristics by using multiparametric and multiregional MR imaging features. *Radiology, 281*(3), 907–918.

Kickingereder, P., Burth, S., Wick, A., Götz, M., Eidel, O., Schlemmer, H.-P., et al. (2016b). Radiomic profiling of glioblastoma: Identifying an imaging predictor of patient survival with improved performance over established clinical and radiologic risk models. *Radiology, 280*(3), 880–889.

Klein, M., . Taphoorn, M. J., Heimans, J. J., van der Ploeg, H. M., Vandertop, W. P., Smit, E. F., et al. (2001). Neurobehavioral status and health-related quality of life in newly diagnosed high-grade glioma patients. Journal of Clinical Oncology, 19(20), 4037–4047.

Klein, M., Heimans, J., Aaronson, N., Van der Ploeg, H., Grit, J., Muller, M., et al. (2002). Effect of radiotherapy and other treatment-related factors on mid-term to long-term cognitive sequelae in low-grade gliomas: A comparative study. *The Lancet, 360*(9343), 1361–1368.

Lacroix, M., Abi-Said, D., Fourney, D. R., Gokaslan, Z. L., Shi, W., DeMonte, F., et al. (2001). A multivariate analysis of 416 patients with glioblastoma multiforme: Prognosis, extent of resection, and survival. *Journal of Neurosurgery, 95*(2), 190–198.

Law, M., Young, R. J., Babb, J. S., Peccerelli, N., Chheang, S., Gruber, M. L., et al. (2008). Gliomas: Predicting time to progression or survival with cerebral blood volume measurements at dynamic susceptibility-weighted contrast-enhanced perfusion MR imaging 1. *Radiology, 247*(2), 490–498.

Legler, J. M., Ries, L. A. G., Smith, M. A., Warren, J. L., Heineman, E. F., Kaplan, R. S., et al. (1999). Brain and other central nervous system cancers: Recent trends in incidence and mortality. *Journal of the National Cancer Institute, 91*(16), 1382–1390.

Liu, L., Zhang, H., Rekik, I., Chen, X., Wang, Q., & Shen, D. (2016) Outcome prediction for patient with high-grade gliomas from brain functional and structural networks. In *International Conference on Medical Image Computing and Computer-Assisted Intervention,* 26-34.

Louis, D. N., Ohgaki, H., Wiestler, O. D., Cavenee, W. K., Burger, P. C., Jouvet, A., et al. (2007). The 2007 WHO classification of tumours of the central nervous system. *Acta Neuropathologica, 114*(2), 97–109.

Lowe, D. G. (2004). Distinctive image features from scale-invariant keypoints. *International Journal of Computer Vision, 60*(2), 91–110.

Lynall, M.-E., Bassett, D. S., Kerwin, R., McKenna, P. J., Kitzbichler, M., Muller, U., et al. (2010). Functional connectivity and brain networks in schizophrenia. *Journal of Neuroscience, 30*(28), 9477–9487.

Macyszyn, L., Akbari, H., Pisapia, J. M., Da, X., Attiah, M., Pigrish, V., et al. (2016). Imaging patterns predict patient survival and molecular subtype in glioblastoma via machine learning techniques. *Neuro-Oncology, 18*(3), 417–425.

Maesawa, S., Bagarinao, E., Fujii, M., Futamura, M., Motomura, K., Watanabe, H., et al. (2015). Evaluation of resting state networks in patients with gliomas: Connectivity changes in the unaffected side and its relation to cognitive function. *PLoS One, 10*(2), e0118072.

Maldaun, M. V., Suki, D., Lang, F. F., Prabhu, S., Shi, W., Fuller, G. N., et al. (2004). Cystic glioblastoma multiforme: Survival outcomes in 22 cases. *Journal of Neurosurgery, 100*(1), 61–67.

Mazurowski, M. A., Zhang, J., Peters, K. B., & Hobbs, H. (2014). Computer-extracted MR imaging features are associated with survival in glioblastoma patients. *Journal of Neuro-Oncology, 120*(3), 483–488.

Meinshausen, N., & Bühlmann, P. (2006). High-dimensional graphs and variable selection with the lasso. *The Annals of Statistics*, 1436–1462.

Mikl, M., Marecek, R., Hlustik, P., Pavlicova, M., Drastich, A., Chlebus, P., Brazdil, M., & Krupa, P. (2008). Effects of spatial smoothing on fMRI group inferences. *Magnetic Resonance Imaging, 26*, 490–503.

Nie, D., Zhang, H., Adeli, E., Liu, L., & Shen, D. (2016). 3D deep learning for multi-modal imaging-guided survival time prediction of brain tumor patients. In *International Conference on Medical Image Computing and Computer-Assisted Intervention,* 212–220.

Olson, I. R., Plotzker, A., & Ezzyat, Y. (2007). The enigmatic temporal pole: A review of findings on social and emotional processing. *Brain, 130*(7), 1718–1731.

Ostrom, Q. T., Gittleman, H., Farah, P., Ondracek, A., Chen, Y., Wolinsky, Y., et al. (2013). CBTRUS statistical report: Primary brain and central nervous system tumors diagnosed in the United States in 2006-2010. *Neuro-Oncology, 15*(suppl 2), ii1–ii56.

Phillips, H. S., Kharbanda, S., Chen, R., Forrest, W. F., Soriano, R. H., Wu, T. D., et al. (2006). Molecular subclasses of high-grade glioma predict prognosis, delineate a pattern of disease progression, and resemble stages in neurogenesis. *Cancer Cell, 9*(3), 157–173.

Pope, W. B., Sayre, J., Perlina, A., Villablanca, J. P., Mischel, P. S., & Cloughesy, T. F. (2005). MR imaging correlates of survival in patients with high-grade gliomas. *American Journal of Neuroradiology, 26*(10), 2466–2474.

Rahman, M., Abbatematteo, J., De Leo, E. K., Kubilis, P. S., Vaziri, S., Bova, F., et al. (2017). The effects of new or worsened postoperative neurological deficits on survival of patients with glioblastoma. *Journal of Neurosurgery, 127*(1), 123–131.

Ratey, J. J. (2001). A user's guide to the brain: Perception, attention, and the four theatres of the brain. *Vintage*.

Ricard, D., Idbaih, A., Ducray, F., Lahutte, M., Hoang-Xuan, K., & Delattre, J.-Y. (2012). Primary brain tumours in adults. *The Lancet, 379*(9830), 1984–1996.

Rosazza, C., & Minati, L. (2011). Resting-state brain networks: Literature review and clinical applications. *Neurological Sciences, 32*(5), 773–785.

Rubinov, M., & Sporns, O. (2010). Complex network measures of brain connectivity: Uses and interpretations. *NeuroImage, 52*(3), 1059–1069.

Saksena, S., Jain, R., Narang, J., Scarpace, L., Schultz, L. R., Lehman, N. L., et al. (2010). Predicting survival in glioblastomas using diffusion tensor imaging metrics. *Journal of Magnetic Resonance Imaging, 32*(4), 788–795.

Sawaya, R., Hammoud, M., Schoppa, D., Hess, K. R., Wu, S. Z., Shi, W.-M., et al. (1998). Neurosurgical outcomes in a modern series of 400 craniotomies for treatment of parenchymal tumors. *Neurosurgery, 42*(5), 1044–1055.

Simpson, J. R., Horton, J., Scott, C., Curran, W. J., Rubin, P., et al. (1993). Influence of location and extent of surgical resection on survival of

patients with glioblastoma multiforme: Results of three consecutive radiation therapy oncology group (RTOG) clinical trials. *International Journal of Radiation Oncology, Biology, Physics, 26*(2), 239–244.

Smith, J. S., Chang, E. F., Lamborn, K. R., Chang, S. M., Prados, M. D., Cha, S., et al. (2008). Role of extent of resection in the long-term outcome of low-grade hemispheric gliomas. *Journal of Clinical Oncology, 26*(8), 1338–1345.

Smith, S. M., Miller, K. L., Salimi-Khorshidi, G., Webster, M., Beckmann, C. F., Nichols, T. E., et al. (2011). Network modeling methods for FMRI. *NeuroImage, 54*(2), 875–891.

Sporns, O., Chialvo, D. R., Kaiser, M., & Hilgetag, C. C. (2004). Organization, development and function of complex brain networks. *Trends in Cognitive Sciences, 8*(9), 418–425.

Squire, L., Berg, D., Bloom, F. E., Du Lac, S., Ghosh, A., & Spitzer, N. C. (2012). Fundamental Neuroscience. Academic Press.

Stam, C., Jones, B., Nolte, G., Breakspear, M., & Scheltens, P. (2007). Small-world networks and functional connectivity in Alzheimer's disease. *Cerebral Cortex, 17*(1), 92–99.

Stensjøen, A. L., Solheim, O., Kvistad, K. A., Håberg, A. K., Salvesen, Ø., & Berntsen, E. M. (2015). Growth dynamics of untreated glioblastomas in vivo. *Neuro-Oncology, 17*(10), 1402–1411.

Stupp, R., Dietrich, P.-Y., Kraljevic, S. O., Pica, A., Maillard, I., Maeder, P., et al. (2002). Promising survival for patients with newly diagnosed glioblastoma multiforme treated with concomitant radiation plus temozolomide followed by adjuvant temozolomide. *Journal of Clinical Oncology, 20*(5), 1375–1382.

Stylli, S. S., Kaye, A. H., MacGregor, L., Howes, M., & Rajendra, P. (2005). Photodynamic therapy of high grade glioma–long term survival. *Journal of Clinical Neuroscience, 12*(4), 389–398.

Taphoorn, M., Schiphorst, A. K., Snoek, F., Lindeboom, J., Wolbers, J., Karim, A., et al. (1994). Cognitive functions and quality of life in patients with low-grade gliomas: The impact of radiotherapy. *Annals of Neurology, 36*(1), 48–54.

Tijms, B. M., Wink, A. M., de Haan, W., van der Flier, W. M., Stam, C. J., Scheltens, P., et al. (2013). Alzheimer's disease: Connecting findings from graph theoretical studies of brain networks. *Neurobiology of Aging, 34*(8), 2023–2036.

Tzourio-Mazoyer, N., Landeau, B., Papathanassiou, D., Crivello, F., Etard, O., Delcroix, N., et al. (2002). Automated anatomical labeling of activations in SPM using a macroscopic anatomical parcellation of the MNI MRI single-subject brain. *NeuroImage, 15*(1), 273–289.

van Dellen, E., Douw, L., Hillebrand, A., de Witt Hamer, P. C., Baayen, J. C., Heimans, J. J., et al. (2014). Epilepsy surgery outcome and functional network alterations in longitudinal MEG: A minimum spanning tree analysis. *NeuroImage, 86*, 354–363.

van Dellen, E., Douw, L., Hillebrand, A., Ris-Hilgersom, I. H., Schoonheim, M. M., Baayen, J. C., et al. (2012). MEG network differences between low-and high-grade glioma related to epilepsy and cognition. *PLoS One, 7*(11), e50122.

van Dellen, E., Hillebrand, A., Douw, L., Heimans, J. J., Reijneveld, J. C., & Stam, C. J. (2013). Local polymorphic delta activity in cortical lesions causes global decreases in functional connectivity. *NeuroImage, 83*, 524–532.

Van Den Heuvel, M. P., & Pol, H. E. H. (2010). Exploring the brain network: A review on resting-state fMRI functional connectivity. *European Neuropsychopharmacology, 20*(8), 519–534.

Viola, P., & Jones, M. J. (2004). Robust real-time face detection. *International Journal of Computer Vision, 57*(2), 137–154.

Wang, H., Douw, L., Hernandez, J. M., Reijneveld, J., Stam, C., & Van Mieghem, P. (2010). Effect of tumor resection on the characteristics of functional brain networks. *Physical Review E, 82*(2), 021924.

Wang, J., Wang, X., Xia, M., Liao, X., Evans, A., & He, Y. (2015a). GRETNA: A graph theoretical network analysis toolbox for imaging connectomics. *Frontiers in Human Neuroscience, 9*, 386.

Wang, J., Wang, L., Zang, Y., Yang, H., Tang, H., Gong, Q., Chen, Z., Zhu, C., & He, Y. (2009a). Parcellation-dependent small-world brain functional networks: A resting-state fMRI study. *Human Brain Mapping, 30*(5), 1511–1523.

Wang, L., Zhu, C., He, Y., Zang, Y., Cao, Q., Zhang, H., et al. (2009b). Altered small-world brain functional networks in children with attention-deficit/hyperactivity disorder. *Human Brain Mapping, 30*(2), 638–649.

Wang, Y., Wang, K., Li, S., Wang, J., Ma, J., Jiang, T., et al. (2015b). Patterns of tumor contrast enhancement predict the prognosis of anaplastic gliomas with IDH1 mutation. *American Journal of Neuroradiology, 36*(11), 2023–2029.

Wee, C. Y., Yap, P. T., Denny, K., Browndyke, J. N., Potter, G. G., Welsh-Bohmer, K. A., ... & Shen, D. (2012). Resting-state multi-spectrum functional connectivity networks for identification of MCI patients. *PLoS One, 7*(5), e37828.

Wee, C.-Y., Yang, S., Yap, P.-T., Shen, D., & Initiative, A. s. D. N. (2016). Sparse temporally dynamic resting-state functional connectivity networks for early MCI identification. *Brain Imaging and Behavior, 10*(2), 342–356.

Wu, J.-S., Zhou, L.-F., Tang, W.-J., Mao, Y., Hu, J., Song, Y.-Y., et al. (2007). Clinical evaluation and follow-up outcome of diffusion tensor imaging-based functional neuronavigation: A prospective, controlled study in patients with gliomas involving pyramidal tracts. *Neurosurgery, 61*(5), 935–949.

Xia, M., Wang, J., & He, Y. (2013). BrainNet viewer: A network visualization tool for human brain connectomics. *PLoS One, 8*(7), e68910.

Xu, H., Ding, S., Hu, X., Yang, K., Xiao, C., Zou, Y., et al. (2013). Reduced efficiency of functional brain network underlying intellectual decline in patients with low-grade glioma. *Neuroscience Letters, 543*, 27–31.

Yu, Z., Tao, L., Qian, Z., Wu, J., Liu, H., Yu, Y., et al. (2016a). Altered brain anatomical networks and disturbed connection density in brain tumor patients revealed by diffusion tensor tractography. *International Journal of Computer Assisted Radiology and Surgery, 11*(11), 2007–2019.

Yu, R., Zhang, H., An, L., Chen, X., Wei, Z., & Shen, D. (2016b). Correlation-weighted sparse group representation for brain network construction in MCI classification. In *International Conference on Medical Image Computing and Computer-Assisted Intervention,* 37-45.

Zacharaki, E. I., Morita, N., Bhatt, P., O'rourke, D., Melhem, E., & Davatzikos, C. (2012). Survival analysis of patients with high-grade gliomas based on data mining of imaging variables. *American Journal of Neuroradiology, 33*(6), 1065–1071.

Zalesky, A., Fornito, A., Harding, I. H., Cocchi, L., Yücel, M., Pantelis, C., & Bullmore, E. T. (2010). Whole-brain anatomical networks: Does the choice of nodes matter? *NeuroImage, 50*(3), 970–983.

Zhang, D., Johnston, J. M., Fox, M. D., Leuthardt, E. C., Grubb, R. L., Chicoine, M. R., et al. (2009). Preoperative sensorimotor mapping in brain tumor patients using spontaneous fluctuations in neuronal activity imaged with fMRI: Initial experience. *Neurosurgery, 65*(6 Suppl), 226.

Zhang, H., Chen, X., Shi, F., Li, G., Kim, M., Giannakopoulos, P., et al. (2016). Topographical information-based high-order functional connectivity and its application in abnormality detection for mild cognitive impairment. *Journal of Alzheimer's Disease, 54*(3), 1095–1112.

Zhang, H., Chen, X., Zhang, Y., & Shen, D. (2017a). Test-retest reliability of "high-order" functional connectivity in young healthy adults. *Frontiers in Neuroscience, 11*, 439.

Zhang, L., Wang, Q., Gao, Y., Li, H., Wu, G., & Shen, D. (2017b). Concatenated spatially-localized random forests for hippocampus labeling in adult and infant MR brain images. *Neurocomputing, 229*, 3–12.